frontiers in Earth Science

ORIGINAL RESEARCH
published: 02 February 2022
doi: 10.3389/feart.2022.811339

Deep External Fluid Source Along the Gubbio Normal Fault (Italy): Implications for Slip Along the Altotiberina Active Low-Angle Normal Fault System

Hannah Riegel[1]*, *Gabriele Casale*[1], *Francesco Mirabella*[2], *Ethan Hyland*[3] and *Lorenzo Talegalli*[2]

[1]Department of Geological and Environmental Sciences, Appalachian State University, Boone, NC, United States, [2]Dipartimento di Fisica e Geologia, Università degli Studi di Perugia, Perugia, Italy, [3]Department of Marine, Earth, and Atmospheric Sciences, North Carolina State University, Raleigh, NC, United States

Fluids play a critical role in fault slip, fault and damage zone development, and the distribution of seismicity in regional fault systems; however, determining the source of fluids within fault damage zones is complicated by superposition of fluid-related fabrics. Clumped isotopes applied to tectonic studies offer an opportunity to distinguish between fluid sources based on temperature and stable isotopic composition. Here we use the clumped isotope geothermometer and field observations and compare them with microstructural analysis to investigate the Gubbio normal-fault (GuF) core, a major SW-dipping epidetachment fault conjugate to the active Altotiberina low-angle normal fault in central Italy. Several distinct calcite vein sets reveal the incorporation of multiple generations of fluids during development of the damage zone. Clumped isotope results from these various precipitation phases record crystallization temperatures ranging from 87–154°C. These temperatures are broadly consistent with the presence of calcite deformation twin types II and III and are higher than estimates of regional peak burial temperatures. Additionally, stable isotope compositions within vein calcite are distinct from published isotopic values of the Apennine sedimentary succession, which constitutes the local bedrock. We propose that these observations suggest hydrothermal fluids migrated from depths greater than 6 km, which requires hydraulic connectivity along structural pathways between the shallow and deep crust, and fluid overpressures. These fluids reach the GuF via migration along the Altotiberina low-angle normal fault plane and they may be either of diagenetic or of deeper subduction origin. We suggest they possibly originated from the proximal retreating Apennine subduction system, implying that subduction processes exert spatial control on the distribution of fluid-assisted normal faulting and related seismicity which is consistent with the co-migration of closely coupled subduction and hinterland extension in the Apennines from Miocene to Present.

Keywords: normal faults, clumped isotopes, calcite twins, northern apennines, overpressure fluid

OPEN ACCESS

Edited by:
Andrea Billi,
National Research Council (CNR), Italy

Reviewed by:
Luca Aldega,
Sapienza University of Rome, Italy
Sergio Llana-Fúnez,
University of Oviedo, Spain

***Correspondence:**
Hannah Riegel
riegelhb@appstate.edu

Specialty section:
This article was submitted to Structural Geology and Tectonics, a section of the journal Frontiers in Earth Science

Received: *08 November 2021*
Accepted: *10 January 2022*
Published: *02 February 2022*

Citation:
Riegel H, Casale G, Mirabella F, Hyland E and Talegalli L (2022) Deep External Fluid Source Along the Gubbio Normal Fault (Italy): Implications for Slip Along the Altotiberina Active Low-Angle Normal Fault System. Front. Earth Sci. 10:811339. doi: 10.3389/feart.2022.811339

INTRODUCTION

It has been widely recognized that fluids circulate within fault breccia and associated veins and fractures (e.g., Sibson, 1987; Sibson, 1996). In some cases, fractures networks record textural evidence that fluid passage can be episodic and contemporaneous with fault slip (Streit and Cox, 2001; Uysal et al., 2011). In addition, high pressure fluids are important in both faulting, reactivation, and vein formation (Sibson, 1996). These fluids reduce the effective normal stress and facilitate slip on faults in turn promoting the propagation of breccia and fracture networks, and mineralization within fault breccia and vein systems records multiple episodes of fault reactivation as shown by crack-seal mechanisms (Passchier and Trouw, 2005; Nuriel et al., 2011). In this context, microchemical analyses on fault breccia and veins provide information about deformation related fluids (e.g., Kirschner et al., 1993).

Carbonate clumped isotope (Δ_{47}) geothermometry, due to its ability to determine precise calcite crystallization temperatures (e.g., Eiler, 2011), has emerged as a tool for studies of shallow crustal tectonic environments (e.g., Beaudoin et al., 2020; Curzi et al., 2020) particularly when paired with other methods such as calcite twinning geothermometry, U-Pb geochronology, and fluid inclusion microthermometry (e.g., Beaudoin et al., 2020; Curzi et al., 2020). These measurements provide both formation temperature estimates (from Δ_{47}) and source fluid compositions ($\delta^{18}O$, $\delta^{13}C$), thereby providing the means to differentiate meteoric versus deep fluids and examine ascending/descending pathways (e.g., Bergman et al., 2013), as well as delineate generations of cementation and deformation along fault zones (e.g., Hodson et al., 2016). Application of Δ_{47} geothermometry presents a novel opportunity to investigate fluid dynamics and cement generation in fault complexes and fracture zones associated with fault systems where fluid connectivity may play an important role between shallow and deep crustal processes.

Calcite e-twin width and morphology has been correlated with temperature of deformation in naturally deformed calcite (e.g., Burkhard, 1993). For a given amount of twinning, strain mean calcite twin width correlates directly with temperature of deformation such that thin twins dominate up to 170°C and thick twins dominate above 200°C (Ferrill, 1991; Burkhard, 1993; Ferrill, 1998; Ferrill et al., 2004; Passchier and Trouw, 2005). This relationship between twin thickness and temperature has recently been questioned by authors who pointed out that the increasing duration of stress, and hence strain, may cause widening of twin lamellae even at room temperature (Rybacki et al., 2013; Parlangeau et al., 2019). Nevertheless, the optical distinction between different calcite twin type morphology has been successfully applied to tectonic studies where calcite is particularly abundant, especially when coupled with other thermometric techniques (e.g., Meneghini et al., 2012; Musumeci and Vaselli, 2012; Clemenzi et al., 2014; Clemenzi et al., 2015; Marroni et al., 2015; Storti et al., 2018).

The combination of Δ_{47} geothermometry with microstructural analysis on calcite e-twin width and morphology presents an opportunity to investigate fluid dynamics and cement generation in fault complexes and fracture zones associated with fault systems where fluid connectivity may play an important role between shallow and deep crustal processes, such as in the epidetachment faults associated with low angle normal faults. Low-angle (<30°) normal faults (LANFs) are extensional features with a shallow dip that can have horizontal displacements large enough to exhume metamorphic rocks from the middle crust (Davis and Lister, 1988). Normal slip along such low-angle structures is unfavorable according to frictional slip theory (Sibson, 1985), and a number of dynamic models have attempted to reconcile this mechanical paradox geometrically (e.g., rolling hinge; Wernicke and Axen, 1988; Lavier et al., 1999; Mizera et al., 2019). Nonetheless, active slip along low-angle detachments has been observed using seismological and geodetic techniques (e.g., Abers, 1991; Abers et al., 1997; Chiaraluce et al., 2007; Hreinsdóttir and Bennett, 2009) and is feasible when fluid pressures are sufficient to overcome the minimum principal stress (σ_3) (e.g., Sibson, 1985; Sibson, 2000) or when frictionally weak minerals are present within the fault core (Hayman et al., 2003; Numelin et al., 2007; Collettini et al., 2009a, 2009b). Evidence of elevated fluid pressures in the form of mineralized tension gashes and the presence of frictionally weak mineral phases are abundant in exhumed LANFs (e.g., Goodwin, 1999; Manatschal, 1999; Cowan et al., 2003; Isik et al., 2003; Collettini and Holdsworth, 2004) and fluid overpressure is indirectly inferred by modelling (Wawrzyniec et al., 1999; Collettini et al., 2006) and seismological data (Moretti et al., 2009). However, active LANF systems are exceedingly rare, and evidence of high-pressure fluids unambiguously coming from seismogenic depths in the hanging-wall of LANFs far from their breakaway zone is sparse. Epidetachment faults situated within LANF hanging-walls operate in tandem with the detachment and present an opportunity to sample these fluids because they create pathways for overpressured fluids to reach the surface (Reynolds and Lister, 1987; Wawrzyniec et al., 1999).

The Gubbio normal fault (GuF) is a 22 km long SW-dipping normal fault (Barchi, 2002), and the largest of the antithetic epidetachment faults structurally connected to the active Altotiberina low-angle normal fault (ATF) in the northern Apennines, Italy. The ATF is imaged in both the CROP 03 seismic line and commercial seismic profiles (Keller et al., 1994; Barchi et al., 1998b; Mirabella et al., 2004), and is a 70 km long low-angle ENE-dipping extensional detachment active since the early Pliocene (Caricchi et al., 2015). Modern slip along the ATF is observable via microseismicity (Chiaraluce et al., 2007), and geodetic surface velocities (Hreinsdóttir and Bennett, 2009). The GuF intersects the ATF between 4 and 5 km depth and is very well exposed at the surface (De Paola et al., 2006 and therein references). The GuF damage zone contains abundant secondary calcite, filling opening mode fracture sets and slip surfaces. These damage zone calcite veins were previously investigated using fluid inclusions by Bussolotto et al. (2007), who determined that extensional fabrics formed at depths less than 2.5–3 km, in a confined fluid system not related to meteoric water.

We apply carbonate clumped isotope geothermometry and compare them with qualitative calcite twinning observation and microstructural analysis to the GuF damage zone secondary calcite in order to determine fluid source and discuss implications for connectivity between the ATF and

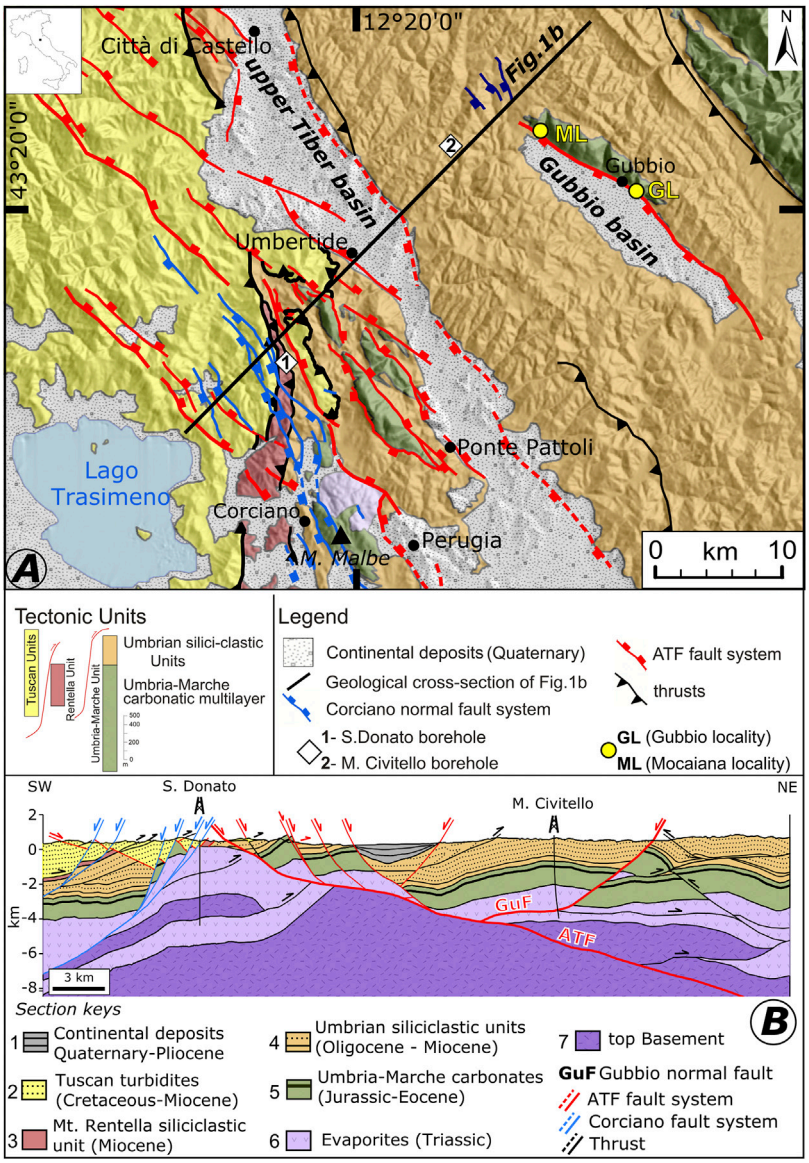

FIGURE 1 | Geologic map **(A)** and cross section **(B)** of the study area. A) Field locations are marked by a yellow circle. Relative to the town of Gubbio, the Mocaiana locality (ML) is to the northwest, the Gubbio locality (GL) is to the southeast. B) The ATF and associated epidetachment faults are denoted in red, while the eastern Corciano fault system is in blue. Modified from Mirabella et al. (2011).

associated epidetachment faults in context of active low-angle normal slip.

GEOLOGIC SETTING

The Northern Apennines are a fold-thrust belt caused by Miocene-Present collision between the Adriatic microplate and European continental margin. This collision is accompanied by an associated retreating syn-convergent subduction system where the coupled compressional foreland and extensional hinterland migrate to the northeast onto the subducting Adria lithosphere (Elter et al., 1975; Reutter et al., 1980; Barchi et al., 1998a). Active extension affects the axial zone of the belt, while the present thrust front is situated off the Adriatic coast of Italy (Boncio and Lavecchia, 2000; De Luca et al., 2009; Chiaraluce et al., 2017). The extensional deformation phase began to affect the western Umbria-Marche Apennines in the early Pliocene (Caricchi et al., 2015), and is parallel with respect to the previous contractional tectonic phase with a minimum principal stress (σ_3) oriented NE-SW. Local modern extension rates, measured by satellite geodesy, are ~2.7 mm/yr (Hreinsdóttir and Bennett, 2009) and accompanied by moderate (Mmax>6.5) normal sense focal mechanism

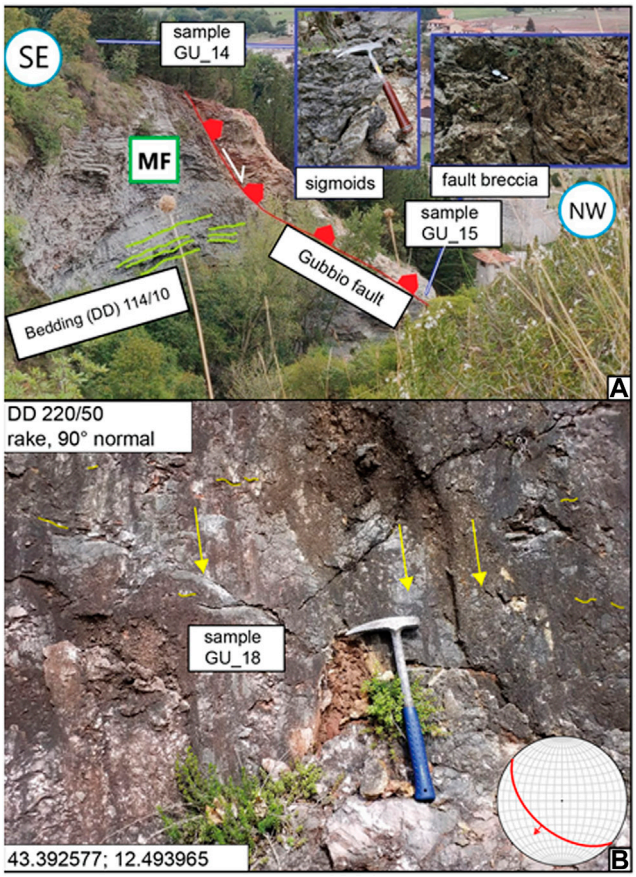

FIGURE 2 | Field sites sampled in this work: **(A)** Gubbio locality (GL), and **(B)** detail of the Mocaiana locality (ML). DD stands for "Dip Direction" notation. MF stands for the Marne a Fucoidi Formation. In the top panel (A), the locations of GU_14 (sigmoids) and GU_15 (fault breccia) are shown. The bottom panel (B) shows the location of sample GU_18.

earthquakes in the shallow crust (Pondrelli et al., 2004; Chiaraluce et al., 2017).

Extension in the northern Apennines is accommodated, in part, by a set of regional low-angle (20°–30°) detachment faults dipping to ENE, which young to the ENE, the youngest and only active of which is the ATF, a ~70 km long structure which borders the upper Tiber Valley (Barchi et al., 1998b; Mirabella et al., 2011; Caricchi et al., 2015). A set of seismogenic antithetic high angle SW-dipping normal faults are situated in the ATF hanging wall (Boncio and Lavecchia, 2000). Among these, the Gubbio normal fault (GuF) crops out 25 km east of the ATF breakaway zone near the town of Gubbio in central Umbria (**Figure 1**). The GuF exposes Meso-Cenozoic carbonate strata belonging to the Umbria-Marche stratigraphic succession (Cresta et al., 1989) in its footwall, and bounds the Gubbio Quaternary continental basin which is situated upon the hanging wall. Based on seismic reflection, the subsurface geometry of the GuF is interpreted to be listric, shallowing to ~10°–15° dip near the intersection with the ATF between 4 and 5 km depth (Mirabella et al., 2004). The maximum displacement of the GuF is ~2.3 km, ~1.5 km of which is attributed to Quaternary extensional slip conjugate to motion along the ATF, based on variation in the thickness of Miocene foredeep deposits across the GuF (Mirabella et al., 2004).

Field Locations

We sampled two locations along the Gubbio Fault (**Figure 1**) for damage zone vein calcite: the Gubbio locality (GL), and the Mocaiana locality (ML) (**Figure 1A**). The GL is situated in the central portion of the fault near the town of Gubbio, where the primary fault surface is well exposed forming a steeply-dipping ~100 m high and ~170 m wide wall. The GL was the focus of the detailed deformation fabric study of Bussolotto et al. (2007) due to the excellent exposure of the damage zone along a road cut that traverses a contiguous transect and extends from the hanging-wall basin sediments through to the damage zone and into the relatively undeformed footwall. At the GL, the exposed footwall includes a substantial portion of the Umbria-Marche carbonate succession representing the upper early Cretaceous to the Eocene section (Marne a Fucoidi, Scaglia Bianca, and Scaglia Rossa formations). This exposed section allows for comprehensive measurement and sampling of the varying styles of damage within these different lithologies, including calcite vein systems and fracture geometries.

The Mocaiana locality (ML) is located approximately 10 km NW of the GL near the northwesternmost surface termination of the GuF. The ML is in a limestone quarry that affords excellent exposure along an approximately 1.1 km transect of the footwall but is limited to the Late Cretaceous Scaglia Group (Scaglia Bianca and Scaglia Rossa) portion of the Umbria-Marche succession involved in the GuF damage zone. At both locations, exposed fault zone tectonites are characterized by foliated gouge through breccia bearing abundant sigmoidal brittle S-C fabrics, and subsidiary fault planes oriented parallel and conjugate to the primary fault surface (**Figure 2**).

MATERIALS AND METHODS

At the GL and ML localities, structural and kinematic data were acquired from multiple outcrops (**Table 1**). At the GL, samples were taken from calcite veins and slicken-lines belonging to the main fault surface and from secondary main-fault-related subsidiary fault planes within the damage zone. Samples from the ML were taken mostly from calcite veins and slicken-lines hosted in the Scaglia Rossa Formation along the main fault plane. Samples were at least 1 cm^3 in size with most between 4 and 7 cm in width to allow for enough material to be used for thin section and clumped isotope analyses.

Laboratory Analyses

We analysed 16 thin sections from two well exposed portions of the GuF (**Figure 1A**) described in the literature (De Paola et al., 2006; Bussolotto et al., 2007), using cathodoluminescence (CL) for texture. Of these, 7 samples were analyzed for Δ_{47} geothermometry (**Table 1**). Temperature estimates based on calcite twin morphology were assessed qualitatively following criteria defined by Burkhard (1993) and additional observations by Ferrill et al. (2004), and are discussed in comparison with Δ_{47} geothermometry data.

TABLE 1 | List of samples collected from the GL and ML localities. Where applicable, observations of vein features and fracture sets, observed calcite twin types and associated temperature values (e.g., Burkhard, 1993; Ferrill et al., 2004), and clumped isotope temperatures are provided. Calcite twin types are grouped morphologically and annotated as follows: Type I and II twins are grouped together as "I/II", Type III twins are separated and denoted as "III". The asterisk (*) indicates samples that were used for clumped isotope analysis.

Locale_Stop#	Sample	Feature	Fracture Set	Twin Type	Temp Range	Δ_{47}
GL_1	GU-4*	Breccia	—	I/II	≤250°C	128°C
43.345001°	GU-14	Sigmoid	—	I/II; III	200–250°C	—
12.596553°	GU-15*	Breccia	—	I/II	≤250°C	109°C
GL_2	GU-1	Vein in limestone	NW-SE; E-W	I/II	≤250°C	—
43.345782°	GU-2	Striae	—	I/II; III	200–250°C	—
12.596669°						
GL_3	GU-3	Breccia	—	I/II; III	200–250°C	—
43.346027°						
12.597023°						
GL_4	N/A	Vein in limestone	NW-SE	—	—	—
43.346288°						
12.597860°						
GL_5	GU-8	Vein in limestone	NW-SE; E-W	I/II	≤250°C	—
43.346585°	GU-9			I/II	≤250°C	—
12.599523°						
GL_6	N/A	Vein in fault core	NW-SE	—	—	—
43.349325°			NE-SW			
12.601241°						
GL_7	GU-11*	Vein in limestone	NW-SE; E-W	I/II	≤250°C	87°C
43.344241°	GU-12*	Striae	—	I/II	≤250°C	106°C
12.597731°	GU-13*	Sigmoid	—	I/II	≤250°C	101°C
ML_1	GU-16*	Breccia	—	I/II	≤250°C	154°C
43.392640°	GU-17*	Sigmoid	—	I/II	≤250°C	152°C
12.493790°	—					
ML_2	GU-18	Sigmoid	—	I/II	≤250°C	—
43.393094°						
12.493355°						
ML_3	GU-19	Vein in limestone	NW-SE	I/II	≤250°C	—
43.387917°						
12.503698°						

Cathodoluminescence

Cathodoluminescence reveals textures not readily visible in plain or cross polarized light with colors and luminescence that are dependent on the distribution of trace minerals within a crystal grain (Pagel et al., 2000). Calcite luminescence is controlled by the distribution of Fe and Mn, which quench and increase luminescence, respectively (Pierson, 1981). Consequently, variation of luminescence in precipitated calcite vein-fill has been interpreted as the result of variable fluid source composition (e.g., Bussolotto et al., 2007). All CL analyses were conducted on a RELION cathodoluminescence microscopy system attached to an Olympus BX-51 petrographic microscope in the Department of Geological and Environmental Sciences at Appalachian State University (ASU). Image acquisition was conducted under 35 millitorr vacuum pressure, 8 kV acceleration voltage, and 0.5 mA beam current, and were processed using Olympus Streamstart 2.3.3 software.

Clumped Isotopes

The carbonate clumped isotope (Δ_{47}) thermometer is based on the theoretical temperature dependence of the abundance of multiply substituted isotopologues containing both ^{13}C and ^{18}O in excess of the stochastic distribution within the solid carbonate phase, which is independent of the isotopic composition of the fluids in which the mineral precipitated. The relative enrichment of clumped isotopologues measured in mass-47 CO_2 (primarily $^{13}C^{18}O^{16}O$) derived from carbonate is known as the Δ_{47} value, and varies with the growth temperature of the sampled carbonate (Ghosh et al., 2006). Thin sections were microsampled and powdered samples were analyzed ($\delta^{18}O$, $\delta^{13}C$, Δ_{47}) in the Paleo^3 Laboratory at North Carolina State University (NCSU). Samples (500–1,500 μg) were digested with phosphoric acid (specific gravity 1.95 g/ml) at 70°C on a Nu Carb automated carbonate device, and resultant CO_2 was cryogenically separated and passed through a Porapak Q trap at -30°C. CO_2 was automatically transferred via dual inlet to a Nu Perspective IS isotope ratio mass spectrometer configured to measure m/z ratios for masses 44–49, which produced $\delta^{18}O$, $\delta^{13}C$, and Δ_{47} values reported relative to the Vienna Peedee Belemnite (VPDB) and the absolute reference frame/Intercarb-carbon dioxide equilibrium scale (ARF/I-CDES; Dennis et al., 2011; Bernasconi et al., 2021). ETH (ETH-1, ETH-2, ETH-3, ETH-4; Bernasconi et al., 2018) solid standards were run concurrently, and data were processed using Easotope software (John and Bowen, 2016) corrected with 70°C acid fractionation (Petersen et al., 2019) and Brand et al. (2010) ^{17}O correction parameters. Replicates with Δ_{48} measurements exceeding ±2‰ were rejected due to contamination by organics/hydrocarbons, and a Pierce Outlier test removed statistical outliers (e.g., Huntington et al., 2009). Standard error was measured using a 95% confidence

interval, and T (Δ_{47}) was calculated using Petersen et al. (2019). Source fluid composition ($\delta^{18}O_{sf}$) was calculated via calcite-water fractionation factor of Kim and O'Neil (1997).

Microstructural Observations

Observation of calcite twin textures allows qualitative estimation of deformation temperature (Burkhard, 1993; Ferrill et al., 2004). Burkhard (1993) describes four twin morphologies (Types I-IV, Burkhard, 1993) that can be correlated to temperature ranges between <170°C to >250°C (Ferrill et al., 2004). Type I twins are straight, < 1 μm thick, and form in up to three sets per grain at temperatures below 200°C. Type II twins are 1–5 μm thick, straight, and form at temperatures ranging from 170–300°C. Type III twins are morphologically distinct from Types I-II, forming thick curved twins at temperatures in excess of 200°C. Type IV twins form at temperatures greater than 250°C as thick patchy trails of small grains. Because twinning in calcite is co-dependent on strain, particularly at low temperatures, Ferrill et al. (2004) describes a more robust quantitative strain and temperature relationship modified from Groshong (1972). Nonetheless, optically distinguishing between calcite twin type morphology provides a useful qualitative tool to estimate temperatures, particularly when coupled with additional thermometric techniques.

Earlier heating during burial of the Umbria-Marche succession in the Apennine foreland likely resulted in calcite twin fabrics. In order to avoid these pre-existing fabrics we focused on deformed crystalline calcite filling veins associated with the damage zone of the GuF described in detail by Bussolotto et al. (2007), which is readily distinguishable from the fossiliferous microcrystalline calcite of the host lithologies.

RESULTS

Field Description

At both sampled locations (GL and ML), the bedding strikes NW, with medium to high density fracturing near areas where distinct brittle-ductile features are observed, such as sigmoids with S-C planes and fault breccia (**Figure 2**; **Table 1**). The predominant fabric is NW-SE trending veins with thicknesses less than 1 cm, comparable to domain Dc-1 in Bussolotto et al. (2007). We also distinguish: 1) E-W trending veins with mostly millimeter scale thickness, and a curvilinear geometry terminating against bedding planes; and 2) NE-SW trending fractures with mm-cm scale thickness which are crosscut by the previously described fracture sets. Stylolites that are predominantly parallel or sub-parallel to bedding, and likely related to burial, are ubiquitous within and outside of the GuF damage zone and have peak heights up to 5 mm. Stylolites associated with tectonic deformation are less common at the outcrop scale but are present along the edges of the sigmoidal foliation fault gouge structures.

Mineral Assemblage

Calcite is the dominant mineral in the clast, matrix, and vein material within all samples, which is consistent with the near ubiquity of limestone in the Umbria-Marche succession. Accessory minerals consisted of 1–10 μm scale baryte, pyrite, and apatite, with very rare zircon and titanite. Clay minerals, predominantly illite, were undetectable except when concentrated as insoluble material along stylolitic surfaces.

Microstructural Observations

Calcite textures from vein material in the GuF contain a range of twinning types (Types I - III; Burkhard, 1993; Ferrill et al., 2004), with most of the samples showing textures of more than one twin type. Each sample exhibits at least faint Type I fabrics, with seven samples strongly exhibiting textures indicative of temperatures >170°C (Type II or greater), and three samples exhibiting textures indicative of temperatures >200°C (Type III fabrics; **Figure 3** and **Table 1**). Cross-cutting features are also evident: Type I twins are consistently cut by Type II and Type III twins in every sample where these types are present. Type II twinning patterns are cut by different generations of Type II, as well as Type I and Type III twinning patterns. In all samples where Type III calcite twinning patterns are found, Type III twins crosscut Type I and Type II; however, we only rarely observed the opposite relationship where Type III twins are crosscut by either Type I or II twins.

Stable and Clumped Isotopes

Stable and clumped isotope analyses were conducted simultaneously on 7 samples from within the damage zone of the GuF at both the GL and ML localities (**Table 1**). Bulk carbon isotope ($\delta^{13}C$) values ranged from +2.2 to +2.5‰ (VPDB) and oxygen isotope ($\delta^{18}O$) values ranged from 0.4 to 8.1‰ (VPDB) (**Figure 4A**). Carbonate clumped isotope (Δ_{47}) values ranged from 0.468 to 0.553‰ (I-CDES), corresponding to temperature estimates of 87–154°C (**Figure 4B**). Calculated source fluid oxygen isotope ($\delta^{18}O_{sf}$) values ranged from +5.3 to +20.5‰ (VSMOW). While there is no apparent trend between bulk isotopic composition and texture or temperature (**Figure 4A**), clumped isotope temperatures do correlate with textural type (and therefore calcite-twinning temperature ranges) and show a trend of substantial $\delta^{18}O_{sf}$ enrichment with higher temperatures (**Figure 4B**), in general agreement with the presence of elevated temperatures as indicated by calcite twinning textures.

DISCUSSION

Fluid Temperature

Temperatures determined from clumped isotopes are in the range of 87–154°C (**Table 1**). Our calcite twinning observations, indicate temperatures in the same range or slightly higher (**Figure 4**). We observe fabrics consistent with temperatures >170°C in all but five samples. However, all samples that contain high temperature textures (Types II-III; Burkhard, 1993) also contain lower temperature fabrics; for example, sample GU-3 has clear Type III fabrics, but also contains Types I and II twins (**Figure 3**). Lower-temperature (<170°C) fabrics are not completely recrystallized but are often crosscut by later vein generations exhibiting higher temperature fabrics (**Figure 3**). We interpret them as multiple generations of deformation through a thermally evolving or dynamic system.

Clumped isotopes, calcite twin textures, and fluid inclusion geothermometric methods all record distinctly different

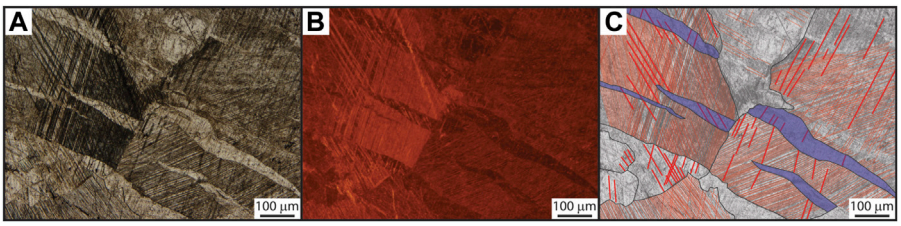

FIGURE 3 | Photomicrograph of deformation vein calcite with twinning. **(A)** plain polarized light (PPL), **(B)** cathodoluminescence, **(C)** annotated PPL image. Panel C annotations include Type I and Type II twins in red, and Type III in blue, approximate grain boundaries are delineated in black. Following the convention of Burkhard (1993) Type I and II twins are relatively thin, straight lines seen in yellow, Type III twins are thick, curved, and tapered. Type I and II twins are cross cut by Type III twins, which rarely also contain straight parallel and relatively thick (>5 µm) tabular likely Type II twins.

temperature estimates. Bussolotto et al. (2007) recognize two distinct temperature ranges, 60–65°C, and 70–80°C, which are both systematically cooler than the clumped isotope T (Δ_{47}) presented here. The discrepancy between these two analytical techniques may be attributed to the nature of these methods. The fluid inclusion study by Bussolotto et al. (2007) targeted intact usable fluid inclusions, which presumably record local crystallization temperatures of single precipitation events during which a portion of the precipitating fluid is entrapped. In fact, Bussolotto et al. (2007) note the abundance of diffused, leaked, and decrepitated inclusions due to overpressure, and the relative scarcity of intact inclusions of sufficient size for analysis. The relative scarcity of available fluid inclusions, and the effect of overpressure may have systematically eliminated fluid inclusions formed during the earlier and deeper record of GuF slip and damage zone development. In contrast, the micro-milling procedure for clumped isotopes in this study likely combines calcite from multiple precipitation phases spanning the entire GuF deformation history. Moreover, solid state reordering of calcite vein material over multiple deformation events may have lowered our temperature estimates following calcite precipitation (e.g., Bonifacie et al., 2012). Our optical and CL observations of multiple cross-cutting vein sets containing an array of deformation temperature fabrics (**Table 1**), and previous interpretations of cross-cutting deformation fabrics (Bussolotto et al., 2007) are consistent with both incorporation of multiple generations of calcite, and post-precipitation solid state isotopic reordering. The result of these processes is that our T (Δ_{47}) temperatures likely reflect some integrated contribution of multiple heating or fluid generations throughout the extensional exhumation of the GuF damage zone. In addition, the micro-milling process may have also introduced some degree of wall rock into our clumped isotope measurements. Previous estimates of maximum burial conditions (and hence temperature) experienced by the Umbria-Marche succession are in the range 80°–100°C as determined by clay mineral assemblage and vitrinite reflectance (Aldega et al., 2007; Corrado et al., 2010). Incorporation of these lower temperature carbonate materials would also reduce our clumped isotope-based temperature estimates; we therefore interpret these T (Δ_{47}) temperatures as minimum estimates of peak fluid temperature.

In contrast, our calcite twin observations suggest temperatures in excess of 170°C in most samples, which is higher than both the fluid inclusion estimates of Bussolotto et al. (2007), and our T (Δ_{47}) estimates. The co-dependence of calcite twin fabrics on strain could possibly result in overestimation of deformation temperatures via textural interpretation, particularly in high strain environments, and previous attempts to quantify this twinning-temperature relationship have relied on calcite deformation fabrics from samples situated away from shear zones (e.g., Ferrill et al., 2004). We therefore consider these texture-based estimates from the GuF damage zone rocks as high-end temperature values, limited by the absence of Type IV twins which have been observed to form at 250°C or above in natural samples (Groshong et al., 1984; Burkhard, 1993; Ferrill and Groshong, 1993). Our combined estimates, nonetheless, point to the abundance of higher temperature fluids, with the highest temperature fluids in the range of ~150–250°C, which suggests a likely deep origin of overpressure fluids.

Fluid Source

We discuss three potential sources for fluids involved in slip and development of damage zone fabrics along the GuF that may be distinguished based on the temperature and isotopic compositions (**Figure 5**). In Scenario 1 (pink, **Figure 5**) meteoric fluid enters the ATF breakaway zone, or percolates down through the hanging-wall blocks, and travels along the ATF fault zone. The ATF fault zone provides a potential pathway as it forms the boundary between metamorphic basement rocks and the sedimentary Umbria-Marche succession, and is likely hosted in a wide permeable damage zone associated with ATF low-angle fault plane. Fluids migrate down dip along the ATF detachment, encountering the GuF at approximately 4–5 km depth as imaged in the CROP-03 seismic line and interpreted by Mirabella et al. (2004), and subsequently travel up the GuF damage zone.

In Scenario 2 (blue, **Figure 5**) meteoric water percolates through the ATF/GuF hanging-wall, enters the GuF damage zone directly, and ascends along the fault. In both Scenarios 1 and 2, fluid stable isotopic compositions would reflect an open fluid system and a combination of conserved meteoric and host rock isotopic sources. Vein composition provides bulk isotopic ($\delta^{18}O$, $\delta^{13}C$) and calculated $\delta^{18}O_{sf}$ values which can be used to distinguish fluid sources; a meteoric fluid source would result in a conserved meteoric composition, or within the range of an

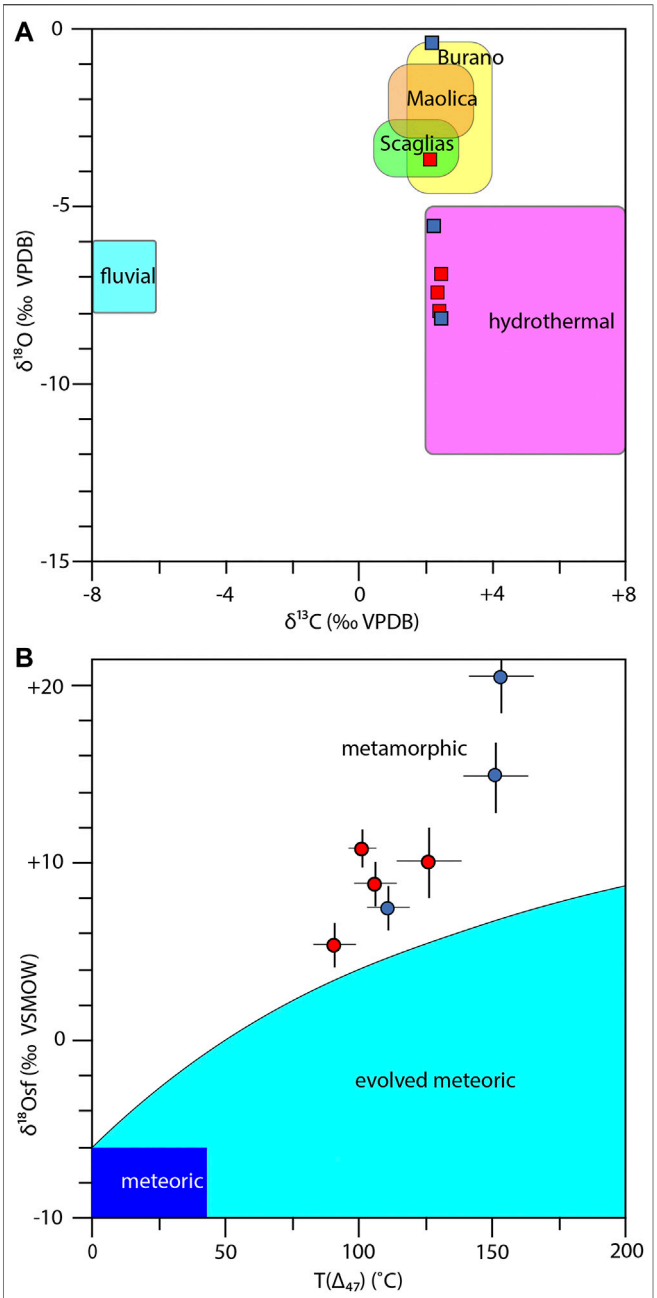

FIGURE 4 | Bulk isotopic composition **(A)** and carbonate clumped isotope temperatures (T [Δ47]) versus calculated fluid composition (δ18Osf) **(B)** of sampled carbonates and regional sources. Colors indicate corresponding twin type (Type I and Type II; red, Type III; blue). The Scaglias, Maolica, Massiccio, and Burano fields are compositions of local marine carbonate (5. Umbria-Marche carbonates, **Figure 1A**; e.g., Morettini et al., 2002; Bussolotto et al., 2007) and evaporite (6. Evaporites, **Figure 1A**; e.g., Lugli, 2001) host rock formations.

intermediate to evolved composition generated via interaction with bedrock (e.g., Hodson et al., 2016; Luetkemeyer et al., 2016). An intermediate to evolved fluid source would be characterized by 1) $\delta^{13}C$ values between surface water, or shallowly degassed CO_2 (a more depleted fluid source; Chiodini et al., 2004), and a host-rock composition (**Figure 4A**), and 2) $\delta^{18}O$ values evolved via temperature and water-rock interactions in an open system (e.g., Luetkemeyer et al., 2016) from a meteoric composition (**Figure 4B**). In Scenario 1, in which meteoric water penetrates to the depth of the GuF and ATF damage zone intersection, the isotopic signature would likely reflect a more evolved composition as isotopic exchange with the host rock would be assisted by an increased temperature at depth. Whereas in Scenario 2, we would expect a maximum temperature corresponding to no more than about 3–4 km (T < 100°C), which is lower than the temperatures measured by clumped isotopes and estimated by calcite twin observations.

Scenario 3 (orange, **Figure 5**), in contrast to Scenarios 1 and 2, includes a closed external deep fluid source rather than a local open meteoric source. In Scenario 3, fluid either originates from down dip along the ATF and migrates up along the detachment fault, or simply from the ATF footwall. In this scenario, precipitated vein calcite from fluids migrating up the GuF would record a hydrothermal/metamorphic stable isotopic composition and likely elevated temperatures in the clumped isotope (T > 100°C) and calcite twinning signatures (Type II and greater). Based on likely meteoric (e.g., IAEA/WMO, 2015) and other surface or bedrock sources for this region (e.g., Bussolotto et al., 2007), measured vein compositions and calculated $\delta^{18}O_{sf}$ values, as well as interpreted temperatures (**Figure 4**), do not fit predictions from either Scenario 1 nor Scenario 2. Instead, our results strongly support a deep and externally-sourced fluid (Scenario 3, **Figure 5**).

Both thermometry techniques yielded fluid temperatures that are consistent with or exceed likely ambient temperature at depth for the GuF (Scenario 1, **Figure 5**) or for the ATF between the breakaway zone and intersection with the GuF (Scenario 2, **Figure 5**). Our lowest T (Δ_{47}) temperature estimates are between 87 and 109°C, while our higher estimates range from 128–154°C. As previously discussed, these values are likely underestimated due to the incorporation of lower temperature wall rock and are substantially lower than estimates based on calcite twin fabrics. Using the published geothermal gradient (20°C/km; Mongelli et al., 1989), and assuming no cooling of the fluid during migration, the minimum depth of the fluid source is approximately 6–7 km. Finally, stable isotope ratios are incompatible with any combination of meteoric (IAEA/WMO, 2015) or local bedrock sources, but are consistent with a hydrothermal or metamorphic source (e.g., Della Porta, 2015; Scenario 3, **Figure 5**). Our results agree with a deeper, non-meteoric fluid source for GuF vein fill as also previously suggested in the same area by other authors on the basis of CO_2 flux measurements (c.f., Chiodini et al., 2004), and isotopic signature (Bussolotto et al., 2007).

This deeply-sourced external fluid could come from a few different regionally-important mechanisms: 1) from the dehydration of clay minerals which can occurs in the observed range of temperatures in fold and thrust belts (e.g., Meneghini et al., 2012); or 2) from deep fluids, for instance CO_2, originating from mantle degassing which ascends through the interconnected network of fractures associated with structural deformation around complex tectonic provinces. During their upward

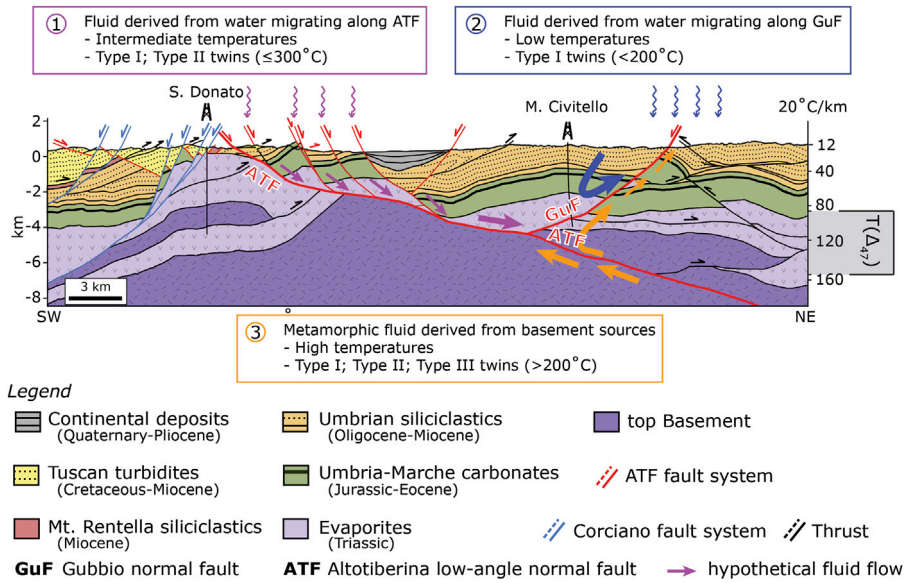

FIGURE 5 | Hypothetical scenarios for fluid source to the GuF. Scenario 1 (pink): meteoric fluid enters the ATF breakaway zone, travels along the detachment, and emerges along the GuF. Scenario 2 (blue): meteoric fluid enters and recirculates along the GuF damage zone fractures. Scenario 3 (orange): hydrothermal metamorphic fluids migrate up the ATF and emerge along the GuF.

migration, these fluids are likely to be entrapped in broad structural barriers like the ATF as previously suggested by other authors (Collettini and Barchi, 2002; Chiodini et al., 2004).

Overpressured Fluids

Deeply-sourced ATF/GuF fluids dominate the isotopic signature, and decrepitation of fluid inclusions (Bussolotto et al., 2007) and calcite-filled hydraulic fractures (Bullock et al., 2014) indicate that fluid pressure can exceed local σ_3. Although hydraulic fracturing in the shallow crust (>3 km) along Andersonian extensional faults (vertical fractures, normal faults dipping between 58° and 68°) can be attributed to lower fluid pressures (Sibson, 2000), the sustained presence of overpressured fluids at greater depth in the ATF system is apparent in model results and geologic observations. Collettini and Barchi (2002) provide a mechanical model for localized slip on the ATF which relies upon the pressure condition where pore-fluid pressure, Pf, exceeds σ_3, attained by entrapment of deep-seated crustal fluids. CO_2 fluid pressure measured in the S. Donato exploration well (**Figure 1** and **Figure 5**) and the Pieve S. Stefano well (50 km NW of S. Donato), which drilled into the ATF footwall, recorded fluid overpressures of ~100 and 70 MPa at depths of 5 and 4 km respectively, corresponding to pore fluid pressures of ~80% of the lithostatic overburden (Collettini et al., 2006).

Craddock et al. (2020) sampled calcite veins present in the GuF footwall in the same GL locality and specifically in the Gubbio fault core (corresponding to our sample GU-15) and determined ^{230}Th–^{234}U–^{238}U ages of 357 ka and 235 ka (Craddock et al., 2020). Their results indicate the presence of recent syn-faulting calcite veins in the Gubbio fault core, suggesting that overpressured fluids have likely been present throughout the Quaternary evolution of the GuF-ATF system.

Tectonic Implications

Deeply sourced fluids play an important role in shallow faulting in the Apennines foreland accretionary prism, and the presence of these fluids are recorded in thrust faults exhumed in the extensional hinterland (e.g., Meneghini et al., 2012). Calcite vein fill within the shear zone of the Monte Rentella thrust fault, part of the Umbria-Tuscan domain of the Apennines fold and thrust belt active during Miocene time (Barsella et al., 2009), records an isotopic signature distinct from the host rock, and consistent with a diagenetic or low-grade metamorphic fluid source from deep structural levels in the accretionary prism (Meneghini et al., 2012). Calcite twin fabrics from within that shear zone display Type II twins, which Meneghini et al. (2012), following Burkhard (1993), interpret as indicative of deformation temperatures between 150 and 200°C. These damage zone temperatures are inconsistent with lower regional peak temperatures, which these authors determine to be between 60 and 110°C based on vitrinite reflectance and clay mineral analysis. Meneghini et al. (2012) interpret the disparity between damage zone fluid temperatures and regional peak temperatures as evidence of hot fluid pumping from deep structural levels within the accretionary prism, and influencing near surface faulting.

Subduction drives burial, diagenesis, and metamorphism in the Northern Apennines, and presents a likely source for fluids, which Meneghini et al. (2012) interpret as migrating along permeable fault zones. The close coupling and proximity of active extensional structures with foreland thrust faulting implies that the same fluid source may also play a significant role in extension in the Apennines. The east dipping active ATF is situated within the transition zone between the accretionary foreland and the extensional hinterland, and can be resolved

in seismic reflection data to the brittle ductile transition at approximately 13 km, penetrating the thickened crust of the Apennines accretionary prism (Pauselli et al., 2006). The geometry of the ATF thus provides a spatial link between the GuF and sediments undergoing burial diagenesis and metamorphism in the accretionary prism. Closer to the surface, two boreholes drilled through the ATF encountered elevated CO_2 pressure at the ATF footwall; in contrast, the Civitello borehole (**Figure 5**) sampled the deep ATF hanging-wall did not yield elevated fluid pressures. These contrasting borehole-determined fluid pressures from above and below the detachment suggest that the rocks bounding the ATF are impermeable, forming a fluid migration pathway along the damage zone. Our observations of elevated fluid temperatures, and previous observations of closed source fluids (e.g., Bussolotto et al., 2007) within the GuF suggest that this fault and possibly other epidetachment faults act as conduits for fluid migrating along the ATF from the subduction and related dehydration or metamorphic reactions.

Our conceptual model of the migration path of fluids derived in the accretionary prism emerging to the near surface in the extensional hinterland (**Figure 5**), is a mirror image of the interpretation of Meneghini et al. (2012) but applied to the proximal Apennines extensional hinterland. The tectonic implications of this interpretation are that subduction, and concomitant metamorphism and diagenesis, exert a spatial control on near surface seismicity and the style of extension in the hinterland. Seismicity within the ATF hanging-wall is largely concentrated along faults located closest to the foreland, such as the GuF (Chiaraluce et al., 2017); in contrast, older epidetachment faults (e.g., Corciano fault; **Figure 1B**) are situated far from the source of subduction-related metamorphic fluids and are less active. On a larger scale, our interpretation implies that proximity to the subduction zone moderates the distribution of low-angle normal faulting, which Sibson (1985) suggests is viable provided sufficient fluid pressures. NE migration of large-scale low angle extensional structures such as the ATF has persisted since the Miocene, migrating in tandem with the retreating subduction front, leaving exhumed inactive structures which become progressively older towards the hinterland (Collettini and Holdsworth, 2004). The ATF is the youngest and only active LANF in the Northern Apennines and is the closest to the Apennine foreland; we suggest that its current microseismic activity (Chiaraluce et al., 2007; Chiaraluce et al., 2014) is therefore owed to its proximity to the source of subduction-related fluids.

CONCLUSIONS

Field and micro-scale calcite vein fabrics within the Gubbio Fault damage zone record the pervasive role of fluids during faulting. Our clumped/stable isotopic measurements and microstructural observations are inconsistent with a near-surface source of these fluids. We calculate that fluid temperatures were in some places in excess of 150°C and show that fluid compositions are inconsistent with fluid-rock interaction for any of the lithological units in the ATF hanging-wall, but are instead compatible with a deep external source. We therefore interpret these fluids as deeply sourced fluids and suggest that the structurally-connected ATF is a likely conduit, providing a pathway for fluids derived from processes associated with the nearby Apennine subduction zone. Previous radiometric crystallization ages and borehole fluid pressure measurements suggest that these fluids have persisted within this system throughout at least Quaternary time. This interpretation implies that the proximity of the subduction zone is a key factor in driving low-angle normal faulting and associated epidetachment faulting in the northern Apennines, a conclusion supported by the geologic record of NE migrating low angle normal faulting in the wake of the retreating Apennines subduction zone from the early Miocene to the Present.

DATA AVAILABILITY STATEMENT

The datasets presented in this study can be found in online repositories. The names of the repository/repositories and accession number(s) can be found below: EarthChem database doi:10.26022/IEDA/111720.

AUTHOR CONTRIBUTIONS

All authors participated in the field study and collected samples, and all contributed to manuscript discussions. HR carried out calcite texture analysis and contributed to writing. GC gave guidance for calcite textures and contributed to writing. FM provided regional expertise and contributed to writing. EH carried out clumped/stable isotope analyses and contributed to writing. LT carried out initial field and microstructural studies.

FUNDING

Data collection supported by National Science Foundation Award #1625137 to Appalachian State University and by UniPG Departmental Research Projects RICBAS2019MIRABELLA.

ACKNOWLEDGMENTS

Clumped isotope data is available under the EarthChem database 10.26022/IEDA/111720. Graduate support provided by the University of Perugia. We thank S. Cirilli (Perugia University) for helpful suggestions. We thank two reviewers for their thoughtful comments which helped us improve the article, and Associate Editor Andrea Billi for editorial support.

SUPPLEMENTARY MATERIAL

The Supplementary Material for this article can be found online at: https://www.frontiersin.org/articles/10.3389/feart.2022.811339/full#supplementary-material

REFERENCES

Abers, G. A., Mutter, C. Z., and Fang, J. (1997). Shallow Dips of normal Faults during Rapid Extension: Earthquakes in the Woodlark-D'Entrecasteaux Rift System, Papua New Guinea. *J. Geophys. Res.* 102, 15301–15317. doi:10.1029/97jb00787

Abers, G. A. (1991). Possible Seismogenic Shallow-Dipping normal Faults in the Woodlark-D'Entrecasteaux Extensional Province, Papua New Guinea. *Geol* 19, 1205–1210. doi:10.1130/0091-7613(1991)019<1205:pssdnf>2.3.co;2

Aldega, L., Botti, F., and Corrado, S. (2007). Clay mineral Assemblages and Vitrinite Reflectance in the Laga Basin (Central Apennines, Italy): What Do They Record? *Clays Clay Miner.* 55 (5), 504–518. doi:10.1346/ccmn.2007.0550505

Barchi, M. (2002). Lithological and Structural Controls on the Seismogenesis of the Umbria Region: Observations from Seismic Reflection Profiles. *Boll. Soc. Geol. It.*, 1, 855–864.

Barchi, M., De Feyter, A., Magnani, B., Minelli, G., Pialli, G., and Sotera, B. (1998a). The Structural Style of the Umbria-Marche Fold and Thrust belt. *Memorie della Societa' Geologica Italiana* 52, 557–578.

Barchi, M., Feyter, A. D., Magnani, M. B., Minelli, G., Pialli, G., and Sotera, B. M. (1998b). Extensional Tectonics in the Northern Apennines (Italy): Evidence from the CROP03 Deep Seismic Reflection Line. *Memorie della Societá Geologica Italiana* 52, 528–538.

Barsella, M., Boscherini, A., Botti, F., Marroni, M., Meneghini, F., Motti, A., et al. (2009). Oligocene-Miocene Foredeep Deposits in the Trasimeno Lake Area (Central Italy): Insights in the Evolution of the Northern Apennines. *Ital. J. Geosciences* 128, 341–352. doi:10.3301/IJG.2009.128.2.341

Beaudoin, N., Lacombe, O., Koehn, D., David, M.-E., Farrell, N., and Healy, D. (2020). Vertical Stress History and Paleoburial in Foreland Basins Unravelled by Stylolite Roughness Paleopiezometry: Insights from Bedding-Parallel Stylolites in the Bighorn Basin, Wyoming, USA. *J. Struct. Geology.* 136, 104061. doi:10.1016/j.jsg.2020.104061

Bergman, S. C., Huntington, K. W., and Crider, J. G. (2013). Tracing Paleofluid Sources Using Clumped Isotope Thermometry of Diagenetic Cements along the moab Fault, Utah. *Am. J. Sci.* 313, 490–515. doi:10.2475/05.2013.03

Bernasconi, S. M., Daëron, M., Bergmann, K. D., Bonifacie, M., Meckler, A. N., Affek, H., et al. (2021). A Community Effort to Improve Inter-laboratory Standardization of the Carbonate Clumped Isotope Thermometer Using Carbonate Anchors. *Geochem. Geophys. Geosystems* 22, e2020GC009588. doi:10.1029/2020gc009588

Bernasconi, S. M., Müller, I. A., Bergmann, K. D., Breitenbach, S. F. M., Fernandez, A., Hodell, D. A., et al. (2018). Reducing Uncertainties in Carbonate Clumped Isotope Analysis through Consistent Carbonate-Based Standardization. *Geochem. Geophys. Geosyst.* 19, 2895–2914. doi:10.1029/2017GC007385

Boncio, P., and Lavecchia, G. (2000). A Structural Model for Active Extension in Central Italy. *J. Geodynamics* 29, 233–244. doi:10.1016/S0264-3707(99)00050-2

Bonifacie, M., Calmels, D., and Eiler, J. M. (2012). Clumped Isotope Thermometry of Marbles as an Indicator of the Closure Temperatures of Calcite and Dolomite with Respect to Solid-State Reordering of C–O Bonds. *Mineralogical Mag.* 77, 735. doi:10.1180/minmag.2013.077.5.2

Brand, W. A., Assonov, S. S., and Coplen, T. B. (2010). Correction for the 17O Interference in δ(13C) Measurements when Analyzing CO2 with Stable Isotope Mass Spectrometry (IUPAC Technical Report). *Pure Appl. Chem.* 82, 1719–1733. doi:10.1351/pac-rep-09-01-05

Bullock, R. J., De Paola, N., Holdsworth, R. E., and Trabucho-Alexandre, J. (2014). Lithological Controls on the Deformation Mechanisms Operating within Carbonate-Hosted Faults during the Seismic Cycle. *J. Struct. Geology.* 58, 22–42. doi:10.1016/j.jsg.2013.10.008

Burkhard, M. (1993). Calcite Twins, Their Geometry, Appearance and Significance as Stress-Strain Markers and Indicators of Tectonic Regime: a Review. *J. Struct. Geology.* 15, 351–368. doi:10.1016/0191-8141(93)90132-T

Bussolotto, M., Benedicto, A., Invernizzi, C., Micarelli, L., Plagnes, V., and Deiana, G. (2007). Deformation Features within an Active normal Fault Zone in Carbonate Rocks: The Gubbio Fault (Central Apennines, Italy). *J. Struct. Geology.* 29, 2017–2037. doi:10.1016/j.jsg.2007.07.014

Caricchi, C., Aldega, L., Barchi, M. R., Corrado, S., Grigo, D., Mirabella, F., et al. (2015). Exhumation Patterns along Shallow Low-Angle normal Faults: An Example from the Altotiberina Active Fault System (Northern Apennines, Italy). *Terra Nova* 27, 312–321. doi:10.1111/ter.12163

Chiaraluce, L., Alessandro Amato, A., Simona Carannante, S., Viviana Castelli, V., Marco Cattaneo, M., Massimo Cocco, M., et al. (2014). The Alto Tiberina Near Fault Observatory (Northern Apennines, Italy). *Ann. Geophys.* 57, 1–16. doi:10.4401/ag-6426

Chiaraluce, L., Barchi, M. R., Carannante, S., Collettini, C., Mirabella, F., Pauselli, C., et al. (2017). The Role of Rheology, Crustal Structures and Lithology in the Seismicity Distribution of the Northern Apennines. *Tectonophysics* 694, 280–291. doi:10.1016/j.tecto.2016.11.011

Chiaraluce, L., Chiarabba, C., Collettini, C., Piccinini, D., and Cocco, M. (2007). Architecture and Mechanics of an Active Low-Angle normal Fault: Alto Tiberina Fault, Northern Apennines, Italy. *J. Geophys. Res.* 112, 1–12. doi:10.1029/2007JB005015

Chiodini, G., Cardellini, C., Amato, A., Boschi, E., Caliro, S., Frondini, F., et al. (2004). Carbon Dioxide Earth Degassing and Seismogenesis in central and Southern Italy. *Geophys. Res. Lett.* 31, 1–4. doi:10.1029/2004GL019480

Clemenzi, L., Molli, G., Storti, F., Muchez, P., Swennen, R., and Torelli, L. (2014). Extensional deformation structures within a convergent orogen: The Val di Lima low-angle normal fault system (Northern Apennines, Italy). *J. Struct. Geology.* 66, 205–222. doi:10.1016/j.jsg.2014.05.019

Clemenzi, L., Storti, F., Balsamo, F., Molli, G., Ellam, R., Muchez, P., et al. (2015). Fluid Pressure Cycles, Variations in Permeability, and Weakening Mechanisms along Low-Angle normal Faults: The Tellaro Detachment, Italy. *Geol. Soc. America Bull.* 127, 1689–1710. doi:10.1130/B31203.1

Collettini, C., and Barchi, M. R. (2002). A Low-Angle normal Fault in the Umbria Region (Central Italy): A Mechanical Model for the Related Microseismicity. *Tectonophysics* 359, 97–115. doi:10.1016/S0040-1951(02)00441-9

Collettini, C., De Paola, N., Holdsworth, R. E., and Barchi, M. R. (2006). The Development and Behaviour of Low-Angle normal Faults during Cenozoic Asymmetric Extension in the Northern Apennines, Italy. *J. Struct. Geology.* 28, 333–352. doi:10.1016/j.jsg.2005.10.003

Collettini, C., and Holdsworth, R. E. (2004). Fault Zone Weakening and Character of Slip along Low-Angle normal Faults: Insights from the Zuccale Fault, Elba, Italy. *J. Geol. Soc.* 161, 1039–1051. doi:10.1144/0016-764903-179

Collettini, C., Niemeijer, A., Viti, C., and Marone, C. (2009a). Fault Zone Fabric and Fault Weakness. *Nature* 462, 907–910. doi:10.1038/nature08585

Collettini, C., Viti, C., Smith, S. A. F., and Holdsworth, R. E. (2009b). Development of Interconnected Talc Networks and Weakening of continental Low-Angle normal Faults. *Geology* 37, 567–570. doi:10.1130/g25645a.1

Corrado, S., Aldega, L., and Zattin, M. (2010). Sedimentary vs. Tectonic Burial and Exhumation along the Apennines (Italy). *J. Virtual Explorer* 36. paper 15. doi:10.3809/jvirtex.2009.00232

Cowan, D. S., Cladouhos, T. T., and Morgan, J. K. (2003). Structural Geology and Kinematic History of Rocks Formed along Low-Angle normal Faults, Death Valley, California. *Geo. Soc. Am. Bull.* 115, 1230–1248. doi:10.1130/B25245.1

Craddock, J. P., Malone, D. H., Wartman, J., Kelly, M. J., Junlai, L., Bussolotto, M., et al. (2020). Calcite Twinning Strains from Syn-Faulting Calcite Gouge: Small-Offset Strike-Slip, normal and Thrust Faults. *Int. J. Earth Sci. (Geol Rundsch)* 109, 1–42. Springer Berlin Heidelberg. doi:10.1007/s00531-019-01783-x

Cresta, S., Monechi, S., and Parisi, G. (1989). Stratigrafia del Mesozoico e Cenozoico nell'area umbro-marchigiana. Itinerari geologici sull'Appennino umbro-marchigiano (Italia). *Memorie Descrittive Della Carta Geologica d'Italia* 39, 1–182.

Curzi, M., Aldega, L., Bernasconi, S. M., Berra, F., Billi, A., Boschi, C., et al. (2020). Architecture and Evolution of an Extensionally-Inverted Thrust (Mt. Tancia Thrust, Central Apennines): Geological, Structural, Geochemical, and K-Ar Geochronological Constraints. *J. Struct. Geology.* 136, 104059. doi:10.1016/j.jsg.2020.104059

Davis, G. A., and Lister, G. S. (1988). Detachment Faulting in continental Extension; Perspectives from the Southwestern U.S. Cordillera. *Geol. Soc. America Spec. Paper* 218, 133–160. doi:10.1130/spe218-p133

De Luca, G., Cattaneo, M., Monachesi, G., and Amato, A. (2009). Seismicity in Central and Northern Apennines Integrating the Italian National and Regional Networks. *Tectonophysics* 476, 121–135. doi:10.1016/j.tecto.2008.11.032

De Paola, N., Mirabella, F., Barchi, M. R., and Burchielli, F. (2006). Early Orogenic normal Faults and Their Reactivation during Thrust belt Evolution: the Gubbio

Fault Case Study, Umbria-Marche Apennines (Italy). *J. Struct. Geology.* 28, 1948–1957. doi:10.1016/j.jsg.2006.06.002

Della Porta, G. (2015). "Carbonate Build-Ups in Lacustrine, Hydrothermal and Fluvial Settings: Comparing Depositional Geometry, Fabric Types and Geochemical Signature," in *Microbial Carbonates in Space and Time*. Editors D. Bosence and K. Gibbons (London, United Kingdom: Geological Society of London Special Publication), 418, 17–68. doi:10.1144/sp418.4

Dennis, K.J., Affek, H.P., Passey, B.H., Schrage, D.P., and Eiler, J.M. (2011). Defining an absolute reference frame for 'clumped' isotope studies of CO_2. *Geochimica et Cosmochimica Acta* 75, 7117–7131. doi:10.1016/j.gca.2011.09.025

Eiler, J. M. (2011). Paleoclimate Reconstruction Using Carbonate Clumped Isotope Thermometry. *Quat. Sci. Rev.* 30, 3575–3588. doi:10.1016/j.quascirev.2011.09.001

Elter, P., Giglia, G., Tongiorgi, M., and Trevisan, L. (1975). Tensional and Compressional Areas in the Recent (Tortonian to Present) Evolution of the Northern Apennines. *Bollettino di Geofisica Teorica e Applicata* 17, 3–18.

Ferrill, D. A. (1991). Calcite Twin Widths and Intensities as Metamorphic Indicators in Natural Low-Temperature Deformation of limestone. *J. Struct. Geology.* 13, 667–675. doi:10.1016/0191-8141(91)90029-I

Ferrill, D. A. (1998). Critical Re-evaluation of Differential Stress Estimates from Calcite Twins in Coarse-Grained limestone. *Tectonophysics* 285 (1–2), 77–86. doi:10.1016/S0040-1951(97)00190-X

Ferrill, D. A., and Groshong, R. H., Jr (1993). Kinematic Model for the Curvature of the Northern Subalpine Chain, France. *J. Struct. Geology.* 15 (3-5), 523–541. doi:10.1016/0191-8141(93)90146-2

Ferrill, D. A., Morris, A. P., Evans, M. A., Burkhard, M., Groshong, R. H., and Onasch, C. M. (2004). Calcite Twin Morphology: A Low-Temperature Deformation Geothermometer. *J. Struct. Geology.* 26, 1521–1529. doi:10.1016/j.jsg.2003.11.028

Ghosh, P., Adkins, J., Affek, H., Balta, B., Guo, W., Schauble, E.A., Schrag, D., and Eiler, J.M. (2006). ^{13}C–^{18}O Bonds in Carbonate Minerals: A New Kind of Paleothermometer. *Geochimica et Cosmochimica Acta* 70, 1439–1456. doi:10.1016/j.gca.2005.11.014

Goodwin, L. B. (1999). Controls on Pseudotachylyte Formation during Tectonic Exhumation in the South Mountains Metamorphic Core Complex, Arizona. *Geol. Soc. Lond. Spec. Publications* 154, 325–342. doi:10.1144/GSL.SP.1999.154.01.15

Groshong, R. H., Jr (1972). Strain Calculated from Twinning in Calcite. *Geol. Soc. America Bull.* 83 (7), 2025–2038. doi:10.1130/0016-7606(1972)83[2025:scftic]2.0.co;2

Groshong, R. H., Jr, Teufel, L. W., and Gasteiger, C. (1984). Precision and Accuracy of the Calcite Strain-Gage Technique. *Geol. Soc. America Bull.* 95 (3), 357–363. doi:10.1130/0016-7606(1984)95<357:paaotc>2.0.co;2

Hayman, N., Knott, J., Cowan, D. S., Nemser, E., and Sarna-Wojcicki, A. (2003). Quaternary Low Angle Slip on Detachment Faults in Death Valley, California. *Geol. Soc. America Bull.* 31, 343–346. doi:10.1130/0091-7613(2003)031<0343:qlasod>2.0.co;2

Hodson, K. R., Crider, J. G., and Huntington, K. W. (2016). Temperature and Composition of Carbonate Cements Record Early Structural Control on Cementation in a Nascent Deformation Band Fault Zone: Moab Fault, Utah, USA. *Tectonophysics* 690, 240–252. doi:10.1016/j.tecto.2016.04.032

Hreinsdottir, S., and Bennett, R. A. (2009). Active Aseismic Creep on the Alto Tiberina Low-Angle normal Fault, Italy. *Geology* 37, 683–686. doi:10.1130/G30194A.1

Hsu, K.J., Cita, M. B., and Ryan, W. B. F. (1973). The Origin of the Mediterranean Evaporite: DSDP Deep Sea Drilling Project, Initial Reports of the Deep Sea Drilling Project, Covering Leg 13 of the Cruises of the Drilling Vessel Glomar Challenger Lisbon, Portugal to Lisbon, Portugal. 43, 1202–1231. doi:10.2973/dsdp.proc.13.143.1973

Huntington, K. W., Eiler, J. M., Affek, H. P., Guo, W., Bonifacie, M., Yeung, L. Y., et al. (2009). Methods and Limitations of 'clumped' CO2isotope (Δ47) Analysis by Gas-Source Isotope Ratio Mass Spectrometry. *J. Mass. Spectrom.* 44, 1318–1329. doi:10.1002/jms.1614

IAEA/WMO (2015). Global Network of Isotopes in Precipitation. The GNIP Database. Available at: https://nucleus.iaea.org/wiser. Accessesd July 2020.

Isik, V., Seyitoğlu, G., and Çemen, I. (2003). Ductile-brittle Transition along the Alaşehir Detachment Fault and its Structural Relationship with the Simav Detachment Fault, Menderes Massif, Western Turkey. *Tectonophysics* 374, 1–18. doi:10.1016/S0040-1951(03)00275-0

John, C. M., and Bowen, D. (2016). Community Software for Challenging Isotope Analysis: First Applications of 'Easotope' to Clumped Isotopes. *Rapid Commun. Mass. Spectrom.* 30, 2285–2300. doi:10.1002/rcm.7720

Keller, J. V. A., Minelli, G., and Pialli, G. (1994). Anatomy of Late Orogenic Extension: The Northern Apennines Case. *Tectonophysics* 238, 275–294. doi:10.1016/0040-1951(94)90060-4

Kim, S.-T., and O'Neil, J. R. (1997). Equilibrium and Nonequilibrium Oxygen Isotope Effects in Synthetic Carbonates. *Geochimica et Cosmochimica Acta* 61, 3461–3475. doi:10.1016/S0016-7037(97)00169-5

Kirschner, D. L., Sharp, Z. D., and Teyssier, C. (1993). Vein Growth Mechanisms and Fluid Sources Revealed by Oxygen Isotope Laser Microprobe. *Geol* 21 (1), 85–88. doi:10.1130/0091-7613(1993)021<0085:vgmafs>2.3.co;2

Lavier, L. L., Roger Buck, W., and Poliakov, A. N. B. (1999). Self-consistent Rolling-Hinge Model for the Evolution of Large-Offset Low-Angle normal Faults. *Geol* 27, 1127–1130. doi:10.1130/0091-7613(1999)027<1127:scrhmf>2.3.co;2

Luetkemeyer, P. B., Kirschner, D. L., Huntington, K. W., Chester, J. S., Chester, F. M., and Evans, J. P. (2016). Constraints on Paleofluid Sources Using the Clumped-Isotope Thermometry of Carbonate Veins from the SAFOD (San Andreas Fault Observatory at Depth) Borehole. *Tectonophysics* 690, 174–189. doi:10.1016/j.tecto.2016.05.024

Lugli, S. (2001). Timing of post-depositional Events in the Burano Formation of the Secchia valley (Upper Triassic, Northern Apennines), Clues from gypsum-anhydrite Transitions and Carbonate Metasomatism. *Sediment. Geology.* 140, 107–122. doi:10.1016/s0037-0738(00)00174-3

Manatschal, G. (1999). Fluid- and Reaction-Assisted Low-Angle normal Faulting: Evidence from Rift-Related Brittle Fault Rocks in the Alps (Err Nappe, Eastern Switzerland). *J. Struct. Geology.* 21, 777–793. doi:10.1016/S0191-8141(99)00069-3

Marroni, M., Pandolfi, L., Catanzariti, R., and Catanzariti, R. (2015). Updated Picture of the Ligurian and Sub-ligurian Units in the Mt. Amiata Area (Tuscany, Italy): Elements for Their Correlation in the Framework of the Northern Apennines. *Ijg* 134 (2), 200–218. doi:10.3301/ijg.2014.47

Meneghini, F., Botti, F., Aldega, L., Boschi, C., Corrado, S., Marroni, M., et al. (2012). Hot Fluid Pumping along Shallow-Level Collisional Thrusts: The Monte Rentella Shear Zone, Umbria Apennine, Italy. *J. Struct. Geology.* 37, 36–52. doi:10.1016/j.jsg.2012.02.004

Mirabella, F., Brozzetti, F., Lupattelli, A., and Barchi, M. R. (2011). Tectonic Evolution of a Low-Angle Extensional Fault System from Restored Cross-Sections in the Northern Apennines (Italy). *Tectonics* 30, 1–23. doi:10.1029/2011TC002890

Mirabella, F., Ciaccio, M. G., Barchi, M. R., and Merlini, S. (2004). The Gubbio normal Fault (Central Italy): Geometry, Displacement Distribution and Tectonic Evolution. *J. Struct. Geology.* 26, 2233–2249. doi:10.1016/j.jsg.2004.06.009

Mizera, M., Little, T. A., Biemiller, J., Ellis, S., Webber, S., and Norton, K. P. (2019). Structural and Geomorphic Evidence for Rolling-Hinge Style Deformation of an Active Continental Low-Angle Normal Fault, SE Papua New Guinea. *Tectonics* 38 (5), 1556–1583. doi:10.1029/2018TC005167

Mongelli, F., Zito, G., Ciaranfi, N., and Pieri, P. (1989). Interpretation of Heat Flow Density of the Apennine Chain, Italy. *Tectonophysics* 164, 267–280. doi:10.1016/0040-1951(89)90020-6

Moretti, M., De Gori, P., and Chiarabba, C. (2009). Earthquake Relocation and Three-dimensionalVpandVp/Vsmodels along the Low Angle Alto Tiberina Fault (Central Italy): Evidence for Fluid Overpressure. *Geophys. J. Int.* 176, 833–846. doi:10.1111/j.1365-246X.2008.03984.x

Morettini, E., Santantonio, M., Bartolini, A., Cecca, F., Baumgartner, P. O., and Hunziker, J. C. (2002). Carbon Isotope Stratigraphy and Carbonate Production during the Early-Middle Jurassic: Examples from the Umbria-Marche-Sabina Apennines (central Italy). *Palaeogeogr. Palaeoclimatol. Palaeoecol.* 184, 251–273. doi:10.1016/s0031-0182(02)00258-4

Musumeci, G., and Vaselli, L. (2012). Neogene Deformation and Granite Emplacement in the Metamorphic Units of Northern Apennines (Italy): Insights from Mylonitic Marbles in the Porto Azzurro Pluton Contact Aureole (Elba Island). *Geosphere* 8 (2), 470–490. doi:10.1130/GES00665.1

Numelin, T., Marone, C., and Kirby, E. (2007). Frictional Properties of Natural Fault Gouge from a Low-Angle normal Fault, Panamint Valley, California. *Tectonics* 26, 1–14. doi:10.1029/2005TC001916

Nuriel, P., Rosenbaum, G., Uysal, I. T., Zhao, J.-X., Golding, S., Ram, W., et al. (2011). Formation of Fault-Related Calcite Precipitates and Their Implications for Dating Fault Activity in the East Anatolian and Dead Sea Fault Zones, Geology of the Earthquake Source: A Volume in Honour of Rick Sibson. *Geol. Soc. Lond. Spec. Publications* 359, 229–248. doi:10.1144/sp359.13

Pagel, M., Barbin, P., Blanc, P., and Ohnenstetter, D. (2000). Cathodoluminescence in Geosciences: An Introduction. In: Editors M. Pagel, V. Barbin, P. Blanc, and D. Ohnenstetter. (Springer: Berlin, Heidelberg). doi:10.1007/978-3-662-04086-7_1

Parlangeau, C., Dimanov, A., Lacombe, O., Hallais, S., and Daniel, J.-M. (2019). Uniaxial Compression of Calcite Single Crystals at Room Temperature: Insights into Twinning Activation and Development. *Solid Earth* 10 (1), 307–316. doi:10.5194/se-10-307-2019

Passchier, C. W., and Trouw, R. A. J. (2005). *Microtectonics* (2nd, rev.enl. ed). Berlin; New York: Springer

Pauselli, C., Barchi, M. R., Federico, C., Magnani, M. B., and Minelli, G. (2006). The Crustal Structure of the Northern Apennines (Central Italy): an Insight by the CROP03 Seismic Line. *Am. J. Sci.* 306 (6), 428–450. doi:10.2475/06.2006.02

Petersen, S. V., Defliese, W. F., Saenger, C., Daëron, M., Huntington, K. W., John, C. M., et al. (2019). Effects of Improved ^{17}O Correction on Interlaboratory Agreement in Clumped Isotope Calibrations, Estimates of mineral-specific Offsets, and Temperature Dependence of Acid Digestion Fractionation. *Geochem. Geophys. Geosystems* 20, 3496–3519. doi:10.1029/2018gc008127

Pierson, B.J. (1981). The Control of Cathodoluminescence in Dolomite by Iron and Manganese. *Sedimentology* 28, 601–610. doi:10.1111/j.1365-3091.1981.tb01924.x

Pondrelli, S., Morelli, A., and Ekström, G. (2004). European-mediterranean Regional Centroid-Moment Tensor Catalog: Solutions for Years 2001 and 2002. *Phys. Earth Planet. Interiors* 145, 127–147. doi:10.1016/j.pepi.2004.03.008

Reutter, K. G., Giese, P., and Closs, H. (1980). Lithospheric Split in the Descending Plate: Observations from the Northern Apennines. *Tectonophysics* 64, 11–19. doi:10.1016/0040-1951(80)90254-1

Reynolds, S. J., and Lister, G. S. (1987). Structural Aspects of Fluid-Rock Interactions in Detachment Zones. *Geol* 15, 362–366. doi:10.1130/0091-7613(1987)15<362:saofii>2.0.co;2

Rybacki, E., Evans, B., Janssen, C., Wirth, R., and Dresen, G. (2013). Influence of Stress, Temperature, and Strain on Calcite Twins Constrained by Deformation Experiments. *Tectonophysics* 601, 20–36. doi:10.1016/j.tecto.2013.04.021

Sibson, R. H. (1985). A Note on Fault Reactivation. *J. Struct. Geology.* 7, 751–754. doi:10.1016/0191-8141(85)90150-6

Sibson, R. H. (1987). Earthquake Rupturing as a Mineralizing Agent in Hydrothermal Systems. *Geology* 15 (8), 791. doi:10.1130/0091-7613(1987)15<701:eraama>2.0.co;2

Sibson, R. H. (2000). Fluid Involvement in normal Faulting. *J. Geodynamics* 29, 469–499. doi:10.1016/S0264-3707(99)00042-3

Sibson, R. H. (1996). Structural Permeability of Fluid-Driven Fault-Fracture Meshes. *J. Struct. Geology.* 18 (8), 1031–1042. doi:10.1016/0191-8141(96)00032-6

Storti, F., Balsamo, F., Mozafari, M., Koopman, A., Swennen, R., and Taberner, C. (2018). Syn-contractional overprinting between extension and shortening along the Montagna dei Fiori Fault during Plio-Pleistocene antiformal stacking at the Central Apennines thrust wedge toe. *Tectonics* 37 (10), 3690–3720. doi:10.1029/2018TC005072

Streit, J. E., and Cox, S. F. (2001). Fluid Pressures at Hypocenters of Moderate to Large Earthquakes. *J. Geophys. Res.* 106, 2235–2243. doi:10.1029/2000jb900359

Uysal, I. T., Feng, Y.-x., Zhao, J.-x., Bolhar, R., Işik, V., Baublys, K. A., et al. (2011). Seismic Cycles Recorded in Late Quaternary Calcite Veins: Geochronological, Geochemical and Microstructural Evidence. *Earth Planet. Sci. Lett.* 303 (1–2), 84–96. doi:10.1016/j.epsl.2010.12.039

Wawrzyniec, T., Selverstone, J., and Axen, G. J. (1999). Correlations between Fluid Composition and Deep-Seated Structural Style in the Footwall of the Simplon Low-Angle normal Fault, Switzerland. *Geol* 27, 715–718. doi:10.1130/0091-7613(1999)027<0715:cbfcad>2.3.co;2

Wernicke, B., and Axen, G. J. (1988). On the Role of Isostasy in the Evolution of normal Fault Systems. *Geol* 16, 848–851. doi:10.1130/0091-7613(1988)016<0848:otroii>2.3.co;2

Yu, Z., Beilman, D. W., and Jones, M. C. (2009). Sensitivity of Northern Peatland Carbon Dynamics to Holocene Climate Change. Carbon Cycling in Northern Peatlands. *Geophysical Monograph Series* 184, –. doi:10.1029/2008GM000822

Conflict of Interest: The authors declare that the research was conducted in the absence of any commercial or financial relationships that could be construed as a potential conflict of interest.

Publisher's Note: All claims expressed in this article are solely those of the authors and do not necessarily represent those of their affiliated organizations, or those of the publisher, the editors, and the reviewers. Any product that may be evaluated in this article, or claim that may be made by its manufacturer, is not guaranteed or endorsed by the publisher.